ELSEVIER

Composites: Part A 30 (1999) 531–536

composites
Part A: applied science and manufacturing

Micromechanics modeling of smart composites

Minoru Taya*

Department of Mechanical Engineering, University of Washington, Box 352600, Seattle, WA 98195, USA

Abstract

This paper discusses a summary of analytical modeling as applied to selected smart composites which include piezoelectric composites, shape memory alloy (SMA) fiber composites, and piezoresistive composites. First we discuss the definition of 'smart materials' which exhibit coupling among mechanical, thermal and electromagnetic behavior, then the Eshelby's formulations based on a simple algebraic method for predictions of two types of smart composites properties are stated; piezoelectric and SMA composites, followed by the percolation model which is applied to obtain the strain–electric conductivity relations of elastomer composites. The predictions based on these models are shown to be in good agreement with limited experimental results. © 1999 Elsevier Science Ltd. All rights reserved.

Keywords: Smart composites; C. Micromechanics; Modeling; Percolation model; Shape memory alloys

1. Introduction

'Smart composites' should be distinguished from ordinary composites that are for primary use as structural materials with high specific mechanical properties. A smart composite can exhibit a desired function in a given environment, such as control of a desired shape, or induction of desired internal stress and strain. The key element for designing a smart composite is to use as the reinforcement a 'smart material' that exhibits coupled behavior, where the coupling takes place between any combination of mechanical, thermal and electromagnetic behavior. In this paper the coupled behavior of various smart materials will be discussed, followed by micromechanics modeling of several smart composites that consist of smart materials as the key constituents.

2. Coupled behavior

Table 1 summarizes various types of coupled behavior between mechanical, thermal and electromagnetic phenomena [1–5]. The first five rows denote linear coupling behavior between flux vector $\tilde{\Sigma}$ and field vector $\tilde{Z}$ or scalar θ, while the last four are for non-linear or non-colinear coupling behavior. Here we shall discuss only linear coupling, although the case of the shape-memory effect will be discussed briefly within the framework of Eshelby's model in a later section. The constitutive equations for materials with linear coupling are written in algebraic form for simplicity:

$$\begin{Bmatrix} \tilde{T} \\ (6\times1) \\ \tilde{D} \\ (3\times1) \\ \tilde{B} \\ (3\times1) \end{Bmatrix} = \begin{bmatrix} \tilde{C} & \tilde{e}^t & \tilde{a}^t \\ (6\times6) & (6\times3) & (6\times3) \\ \tilde{e} & -\tilde{\epsilon} & \tilde{\xi}^t \\ (3\times6) & (3\times3) & (3\times3) \\ \tilde{a} & \tilde{\xi} & -\tilde{\mu} \\ (3\times6) & (3\times3) & (3\times3) \end{bmatrix} \begin{Bmatrix} \tilde{S} \\ (6\times1) \\ -\tilde{E} \\ (3\times1) \\ -\tilde{H} \\ (3\times1) \end{Bmatrix} + \begin{Bmatrix} \tilde{\lambda} \\ (6\times1) \\ \tilde{P} \\ (3\times1) \\ \tilde{O} \\ (3\times1) \end{Bmatrix} \theta \tag{1}$$

where $\tilde{T}$, $\tilde{D}$ and $\tilde{B}$ are the flux vectors of stress, electric displacement and magnetic flux; $\tilde{S}$, $\tilde{E}$ and $\tilde{H}$ are the field vectors of strain, electric field and magnetic field; and $\tilde{\lambda}$, $\tilde{P}$ and θ are the thermal stress vector, the pyroelectric vector and temperature change, respectively. Eq. (1) can be rewritten as

$$\tilde{\Sigma} = \tilde{E}\cdot\tilde{Z} + \tilde{\pi}\theta \tag{2}$$

where $\tilde{\Sigma}$, $\tilde{Z}$ and θ are the flux vector of the 12×1 matrix, the field vector of the 12×1 matrix and the scalar

* Corresponding author. Tel.: + 1-206-685-2850; fax: + 1-206-685-8047.

1359-835X/99/$ - see front matter
PII: S1359-835X(98)00146-8

Table 1
Coupling behavior

Coupled behavior	Flux vector or field vector, $\tilde{\Sigma}$	Field vector or scalar, $\tilde{Z}$ or θ	Coupling coefficient, E
Piezoelectric	Stress, $\tilde{T}$	Electric field, $\tilde{E}$	e
Thermoelastic	Strain, $\tilde{S}$	Temperature change, θ	a
Pyroelectric	Electric displacement, $\tilde{D}$	Temperature change, θ	p
Piezomagnetic	Stress, $\tilde{T}$	Magnetic field, $\tilde{H}$	a
Magnetoelectric	Electric displacement, $\tilde{D}$	Magnetic field, $\tilde{H}$	x
Magnetostrictive	Strain, $\tilde{S}$	Magnetization, $\tilde{M}$	Non-linear
Electrostrictive	Strain, $\tilde{S}$	Electric field, $\tilde{E}$	Non-linear
Piezoresistivity	Electric current density, $\tilde{j}$	Electric field, $\tilde{E}$	s (non-linear in $\tilde{S}$)
Shape-memory effect	Stress, $\tilde{T}$	Temperature change, θ	$T = f(\tilde{S}, \theta)$
	Strain, $\tilde{S}$		Non-linear

(temperature); $\tilde{C}$ and $\tilde{\pi}$ are the stiffness property tensor of the 12 × 12 matrix and the thermal coupling vector of the 12 × 1 matrix, respectively. Eq. (2) can be inverted to

$$\tilde{Z} = \tilde{F}\cdot\tilde{\Sigma} + \tilde{\Lambda}\cdot\theta \tag{3}$$

where $\tilde{F}$ and $\tilde{\Lambda}$ are the compliance property tensor of the 12 × 12 matrix and the compliance thermal vector of the 12 × 1 matrix, respectively, and are given by

$$\tilde{F} = \begin{bmatrix} \tilde{s} & \tilde{g}^t & \tilde{\eta}^t \\ (6\times6) & (6\times3) & (6\times3) \\ \tilde{g} & -\tilde{\beta} & \tilde{\nu}^t \\ (3\times6) & (3\times3) & (3\times3) \\ \tilde{\eta} & \tilde{\nu} & -\tilde{\Omega} \\ (3\times6) & (3\times3) & (3\times3) \end{bmatrix}, \qquad \tilde{\Lambda} = \begin{Bmatrix} \tilde{\Delta} \\ (6\times1) \\ \tilde{\gamma} \\ (3\times1) \\ \tilde{O} \\ (3\times1) \end{Bmatrix} \tag{4}$$

From Eqs. (2) and (3) one can obtain the following relationships:

$$\tilde{E}\cdot\tilde{F} = \tilde{I} \tag{5}$$

$$\tilde{E}\cdot\tilde{\Lambda} + \tilde{\pi} = \tilde{0} \tag{6}$$

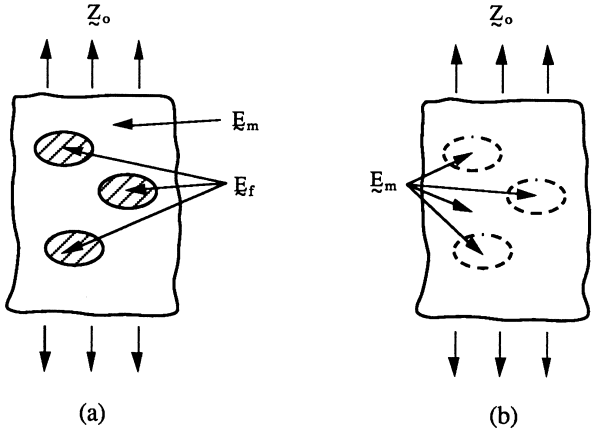

Fig. 1. (a) A composite is subjected to applied field vector $\tilde{Z}_o$; (b) converted to Eshelby's equivalent inclusion problem.

where $\tilde{I}$ is a 12 × 12 identity matrix. From Eqs. (5) and (6), the submatrices in the compliance tensor are interrelated with those in the stiffness tensor matrix. Similarly, $\tilde{\Lambda}$ is related to $\tilde{\pi}$.

3. Micromechanics modeling of a smart composite with linear coupling behavior

Consider a composite which contains numerous fillers made of smart material with linear coupling behavior and is subjected to an applied field vector on the boundary $\tilde{Z}_o$, where temperature is assumed to be constant (Fig. 1(a)). The volume average of the flux and field vectors in each phase are related by

$$\tilde{\Sigma}_c = (1-f)\tilde{\Sigma}_m + f\tilde{\Sigma}_f \tag{7}$$

$$\tilde{Z}_c = (1-f)\tilde{Z}_m + f\tilde{Z}_f \tag{8}$$

where subscripts c, m and f refer to the composite, matrix and fiber phases, respectively, and f is the volume fraction of fillers. The following constitutive equations are valid:

$$\tilde{\Sigma}_i = \tilde{E}_i\cdot\tilde{Z}_i \qquad i = \text{c, m and f} \tag{9}$$

The averaged field vector in the composite, $\tilde{Z}_c$, is equal to the applied field owing to the fact that the disturbance $\tilde{Z}$ field vanishes after integration over the composite domain:

$$\tilde{Z}_c = \frac{1}{V_c}\int_c (\tilde{Z}_o + \tilde{Z})\,dv = \tilde{Z}_o \tag{10}$$

where V_c and dv are the volume of the composite and volume element.

From Eqs. (7)–(10), one arrives at

$$\tilde{E}_c = \tilde{E}_m + f(\tilde{E}_f - \tilde{E}_m)\cdot\tilde{A} \tag{11}$$

where $\tilde{A}$ is the constraint tensor relating the average field in the filler domain to the applied field by

$$\tilde{Z}_f = \tilde{A}\cdot\tilde{Z}_c = \tilde{A}\cdot\tilde{Z}_o \tag{12}$$

$\tilde{A}$ can be obtained by using Eshelby's model, which is given

by

$$\tilde{\Sigma}_o + \tilde{\Sigma} = \tilde{E}_f \cdot (\tilde{Z}_o + \tilde{Z}) = \tilde{E}_m \cdot (\tilde{Z}_o + \tilde{Z} - \tilde{Z}^*) \quad (13)$$

where uniform flux and field vectors are related by

$$\tilde{\Sigma}_o = \tilde{E}_m \cdot \tilde{Z}_o \quad (14)$$

In the above equations, $\tilde{\Sigma}$ and $\tilde{Z}$ are the disturbance of flux and field vectors owing to the existence of the fillers. In Eq. (13) the problem of Fig. 1(a) is converted to the equivalent inclusion problem of Fig. 1(b), where the filler domain is replaced by the equivalent inclusion with eigenfield vector $\tilde{Z}^*$, which is the right-hand side equation in Eq. (13).

The disturbance field vector $\tilde{Z}$ is linearly related to the eigenfield vector $\tilde{Z}^*$ by

$$\tilde{Z} = \tilde{S} \cdot \tilde{Z}^* \quad (15)$$

where $\tilde{S}$ is the Eshelby tensor for the coupling problem and can be expressed in 12×12 matrix form; it is a function of the constituent properties and shape of an ellipsoidal inclusion. It should be noted here that the components of the flux and field vectors in the filler domain become uniform if the shape of the filler is ellipsoidal, facilitating the computation significantly. For non-ellipsoidal fillers, one can still define the averaged Eshelby's tensors within the non-ellipsoidal filler. We examined recently the case of a continuous fiber of *n*-polygon shaped cross-section and defined the average Eshelby's tensor [6]. The field vector in the filler is given by

$$\tilde{Z}_f = \tilde{Z}_o + \tilde{S} \cdot \tilde{Z}^* \quad (16)$$

Rewriting Eq. (13) in terms of $\tilde{Z}_f$ we have

$$\tilde{R}_f \cdot \tilde{Z}_f = \tilde{R}_m (\tilde{Z}_f - \tilde{Z}^*) \quad (17)$$

Eliminating $\tilde{Z}_f$ in Eqs. (16) and (17), one can obtain

$$\left[\tilde{I} + \tilde{S} \cdot \tilde{R}_m^{-1} \cdot (\tilde{R}_f - \tilde{R}_m)\right] \cdot \tilde{Z}_f = \tilde{Z}_o \quad (18)$$

Comparing Eq. (12) with Eq. (18), the constraint tensor $\tilde{A}$ is obtained as

$$\tilde{A}^{dil} = \left[\tilde{I} + \tilde{S} \cdot \tilde{R}^{-1} \cdot (\tilde{R}_f - \tilde{R}_m)\right]^{-1} \quad (19)$$

In the above equations, ' -1' superscript is the inverse of a matrix and 'dil' denotes the solutions for a dilute case of fillers where the interactions among fillers are ignored. When the interactions are considered by the Mori–Tanaka theory [7], the corresponding constraint tensor $\tilde{A}^{MT}$ can be obtained as

$$\tilde{A}^{MT} = \left[(1 - f) + f\tilde{A}^{dil}\right]^{-1} \cdot \tilde{A}^{dil} \quad (20)$$

Thus, the composite stiffness property tensor, $\tilde{E}_c$, can be computed by Eq. (11).

If the flux vector boundary conditions are given, one can similarly arrive at the composite compliance property tensor, $\tilde{F}_c$, which is related to $\tilde{E}_c$ by

$$\tilde{E}_c \cdot \tilde{F}_c = \tilde{I} \quad (21)$$

Eq. (21) is called the 'self-consistency' requirement. Benveniste proved self-consistency for uncoupled behavior of a composite [8].

4. Micromechanics modeling of a smart composite with non-linear coupling

As examples, we shall state below briefly the cases of a composite with shape-memory-alloy fibers and a piezoresistive composite.

4.1. Composite with shape-memory-alloy (SMA) fibers

As far as the macroscopic stresses in a composite with SMA fibers are concerned, we can use Eshelby's model. We have predicted the compressive stress in the matrix material of an SMA composite that was given an initial prestrain ϵ_T at room temperature and then subjected to temperature increase beyond the austenitic finish temperature (A_f). This compressive stress was a dominant contributor to enhancement of the tensile properties of a TiNi SMA fiber/Al matrix composite (stress–strain curve and fatigue resistance) and of a TiNi SMA fiber/epoxy matrix composite (K_{IC}) [9,10]. The compressive stress in the matrix at temperature $\theta \geq A_f$ can be computed by using Eshelby's model for elasto-plastic deformation of a composite. The stress in the TiNi fiber, $\tilde{\sigma}_f$, is given by

$$\tilde{\sigma}_f = \tilde{C}_f \cdot \left(\tilde{e} - \tilde{e}_T - \tilde{e}_p\right) = \tilde{C}_m \cdot (\tilde{e} - \tilde{e}^*) \quad (22)$$

where $\tilde{C}_f$ and $\tilde{C}_m$ are the stiffness tensors of the fiber and matrix materials; $\tilde{e}$, $\tilde{e}_T$, $\tilde{e}_p$ and $\tilde{e}^*$ are the strain disturbance, transformation strain, plastic strain of the fiber and eigenstrain, which has a non-zero value in the fiber domain and vanishes in the matrix, respectively, and where

$$\begin{aligned} \tilde{e}_T &= (\nu_f \epsilon_T,\ \nu_f \epsilon_T,\ -\epsilon_T,\ 0,\ 0,\ 0) \\ \tilde{e}_p &= \left(-\frac{1}{2} e_p,\ -\frac{1}{2} e_p,\ e_p,\ 0,\ 0,\ 0\right) \end{aligned} \quad (23)$$

and

$$\tilde{e} = \tilde{S} \cdot \tilde{e}^* \quad (24)$$

In the above, ν_f, ϵ_T, e_p and $\tilde{S}$ are the Poisson's ratio of the fiber, the prestrain given to the fiber at room temperature, the plastic strain of the fiber axis and Eshelby's tensor, respectively (do not confuse this with strain $\tilde{S}$ used in the previous section). From Eqs. (23) and (24), one can solve for $\tilde{e}^*$ as

$$\tilde{e}^* = \left[(\tilde{C}_f - \tilde{C}_m) \cdot \tilde{S} + \tilde{C}_m\right]^{-1} \cdot \tilde{C}_f \cdot \tilde{e}_p \quad (25)$$

Substituting Eq. (25) into Eq. (22), the fiber stress is computed as

$$\tilde{\sigma}_f = \tilde{C}_m \cdot (\tilde{S} - \tilde{I}) \cdot \left[(\tilde{C}_f - \tilde{C}_m) \cdot \tilde{S} + \tilde{C}_m\right]^{-1} \cdot \tilde{C}_f \cdot \tilde{e}_p \quad (26)$$

The plastic strain in the fiber, $\tilde{e}_p$, can be obtained by

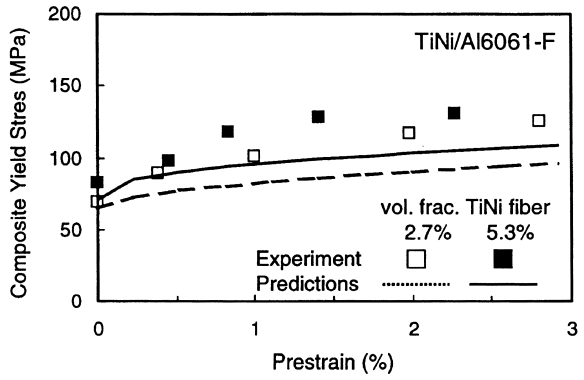

Fig. 2. Composite yield stress dependence on prestrain.

satisfying the yield condition for the fiber:

$$\langle\sigma_f\rangle_{33}-\langle\sigma_f\rangle_{11}=\sigma_{yf} \tag{27}$$

where σ_{yf} is the yield stress of the fiber. Note that σ_{yf} can be interpreted as the stress in the martensitic plateau in the stress–strain curve of the TiNi fiber or any yield stress point beyond the end of the plateau.

Fig. 2 shows the composite yield stress as a function of prestrain ϵ_T for two fiber volume fractions of TiNi shape-memory alloy: $v_f = 0.053$ and 0.027. The predictions (solid lines) based on the present model explain the experimental results [11] reasonably well.

A more complete modeling of one-dimensional SMA behavior has been attempted from the thermodynamic viewpoint by several researchers [12,13].

4.2. Piezoresistive composite

Piezoresistivity can be observed in any conductive or semi-conductive material that can undergo large elongation. Let us consider a circular cylinder rod of length L and cross-sectional area S, with resistivity r. The resistance of the rod, R, is given by

$$R = \rho G \tag{28}$$

$$G = L/S \tag{29}$$

where G is a geometrical parameter. Under applied stress σ, R can be changed by dR [14]

$$\frac{dR}{R} = \left(\frac{1}{\rho}\frac{d\rho}{d\sigma} + \frac{1}{G}\frac{dG}{d\sigma}\right)d\sigma \tag{30}$$

where the first and second terms denote the effect of piezoresistivity and the geometrical factor, respectively, on the overall resistance R. There has been little work on analysis of the piezoresistivity effect in the literature [14]. Recently we examined the piezoresistivity of a conductive short fiber/elastomeric matrix composite [15] both experimentally and theoretically. A brief statement of our analytical model is made in the following.

Let us consider a composite that contains numerous conductive short fibers embedded in an insulating matrix and subjected to applied strain e, see Fig. 3, where (a) and (b) denote the case of formation of a percolation network of conductive short fibers and the degeneration of such a network respectively. The analytical model consists of two parts: (1) a finite deformation model and (2) a fiber percolation model. Fig. 4(a) and (b) illustrate the case of a three-dimensional (3D) affine deformation model before and after a uniaxial strain increment $\Delta\epsilon$ is applied, respectively. Assuming that the initial distribution of fiber orientation angle is random in-plane, it becomes narrower with increasing strain e, which in turn changes the microstructure of the short-fiber network. The electrical conductivity of the ith percolating network along the x axis can then be computed by the following power law:

$$\sigma_{xi} = \sigma_f(p - p_c)^t \tag{31}$$

where p is the probability of bonds and given by [16]

$$p = \frac{N_f + 2N_i}{4N_f + 2N_i} \tag{32}$$

Here σ_f is the conductivity of the fiber; t is a critical exponent dependent only on dimensionality and type of microstructure; p_c is the critical probability of bonds at the percolation threshold, at and above which the composite becomes conductive; and N_f and N_i are the number of fibers and number of intersecting points. The effective electrical conductivity of the composite along the x axis, σ_x, is then computed from

$$\sigma_x = \sum_{i=1}^{m} b_{yi}b_{zi}\sigma_{xi} \tag{33}$$

where m is the number of percolating clusters, and b_{yi} (b_{zi}) is the width of the ith percolating network along the y (z) axis. On the basis of these models and the input data of Table 2 for Ni-coated short graphite fiber/natural rubber composite, we computed the composite conductivity σ_x. The results are

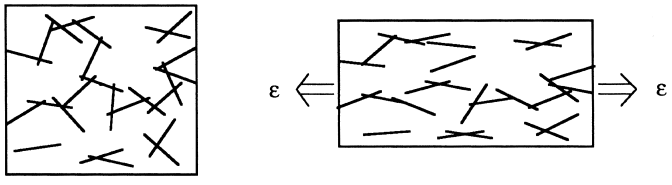

(a) percolating before straining (b) no percolating after straining

Fig. 3. Expected microstructure change under straining: (a) percolation before straining; (b) no percolating after straining.

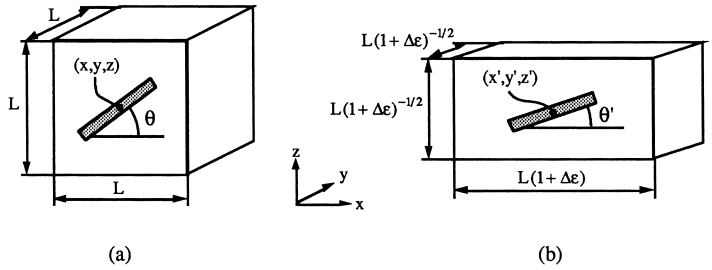

Fig. 4. 3D affine model where only angle θ is shown for illustrative purposes.

Table 2
Input data for computation of electrical conductivity

Sample dimensions	$L_x = 10$ mm, $L_y = 5$ mm, $L_z = 1.5$ mm
Fiber dimensions	$l = 0.825$ mm, $d = 0.015$ mm
Conductivity:	
matrix	1×10^{-17} S/m
fiber	7×10^{4} S/m
Critical bond probability (p_c)	0.44
Critical exponent (t)	1.9
In-plane cut-off angle	20°
Out-of plane cut-off angle	10°

plotted as a solid line in Fig. 5 as a function of applied in-plane strain. The experimental data are also shown in Fig. 5, and a good agreement can be seen between them.

5. Conclusion

Micromechanics modeling for designing a smart composite, where smart materials with coupling behavior are used as reinforcement, is reviewed briefly with the following conclusions.

1. Eshelby's model can be extended to all cases of smart composite design for linear coupling reinforcement.
2. Eshelby's model can still be applicable to the case of non-linear coupling on a limited basis.
3. The problem of electrical conduction in a piezoresistive composite must be solved by using a fiber percolation model.
4. There exists a need to develop new models for the analysis of other non-linear coupling behavior.

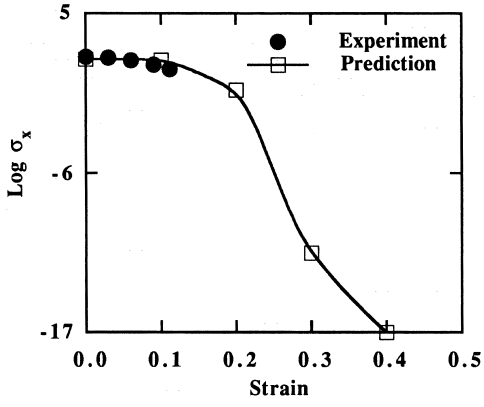

Fig. 5. Comparison between the analytical and experimental results.

Acknowledgements

The present work was supported in part by a grant from the National Science Foundation to the University of Washington (CMS-9414696). The author is also grateful to Dr Y. Furuya of Tohoku University, Professor A. Shimamoto of Saitama Institute of Technology, and Professor K. Ono of Ibaraki University for their help with the experimental work.

References

[1] Taya M. Micromechanics modeling of electronic composites. Trans ASME J Eng Mater Technol 1996;117:462–469.
[2] Landau LD, Lifshitz EM, Pitaevskii LP. Electrodynamics of continuous media, 2nd ed. Landau and Lifshitz course of theoretical physics, vol. 8. Oxford: Pergamon Press, 1984.
[3] Dunn ML, Taya M. An analysis of piezoelectric composite materials containing ellipsoidal inhomogeneity. Proc Roy Soc London 1993;A443:265–287.
[4] Dunn ML. Micromechanics of coupled electroelastic composite: effective thermal expansion and pyroelectric coefficients. J Appl Phys 1993;73(10):5131–5140.
[5] Ikeda T. Fundamentals of piezoelectricity. Oxford: Oxford University Press, 1990.
[6] Nozaki H, Taya M. Stress field in a two-dimensional n-polygon shaped inclusion with uniform eigenstrain. J Appl Mech 1997;64:495–502.
[7] Mori T, Tanaka K. Average stress in matrix and average elastic energy of materials with misfitting inclusions. Acta Metall 1973;21:571–574.
[8] Benveniste Y. A new approach to the application of Mori–Tanaka theory in composite materials. Mech Mater 1987;6:147–157.
[9] Taya M, Shimamoto A, Furuya Y. Design of smart composites based on shape memory effect. In: Poursartip A, Street K, editors. Proc. ICCM-10, Whistler, BC, Canada, August 1995:V275–282.
[10] Furuya Y, Shimamoto A, Taya M. Enhancement of mechanical properties of TiNi fiber composites by shape memory effect. In: Inoue K, Taya M, Shen SI, editors. Proc. First US–Japan Work Shop on Smart Materials & Structures, University of Washington, Seattle, WA, 4–5 December 1995. TMS-AIME, 1997;65–74.
[11] Hamada K, Lee JH, Mizuuchi K, Taya M, Inoue K. Thermomechanical behavior of TiNi shape memory alloy fiber reinforced 6061

aluminum matrix composite. Metall Mater Trans A 1998;29A:1127–1135.

[12] Tanaka K, Nagaki S. A thermomechanical description of materials with internal variables in the process of phase transition. Ingenieur-Archive 1982;51:287–299.

[13] Kamita T, Matsuzaki Y. Pseudoelastic hysteresis of shape memory alloys. In: Inoue K, Taya M, Shen SI, editors. Proc. First US–Japan Work Shop on Smart Materials & Structures, University of Washington, Seattle, WA, 4–5 December 1995. TMS-AIME, 1997; 117–124.

[14] Carmona F, Canet R, Delhaes P. Piezoresistivity of heterogeneous solids. J Appl Phys 1987;61(7):2550–2557.

[15] Taya M, Kim WJ, Ono K. Electro-mechanical coupling behavior of conductive short fiber reinforced elastomer. In: Dunn ML, Taya M, Saka M, editors. Mechanics and materials for electronic packaging, vol. 3: Coupled field behavior in materials. ASME AMD-193, 1994:61–72.

[16] Ueda N, Taya M. Prediction of the electrical conductivity of two-dimensionally misoriented short fiber composites by a percolation model. J Appl Phys 1986;60(1):459–461.